Since January 2020 Elsevier has created a COVID-19 resource centre with free information in English and Mandarin on the novel coronavirus COVID-19. The COVID-19 resource centre is hosted on Elsevier Connect, the company's public news and information website.

Chemical Engineering Journal 439 (2022) 135613

Contents lists available at ScienceDirect

Chemical Engineering Journal

journal homepage: www.elsevier.com/locate/cej

Uncovering the disposable face masks as vectors of metal ions (Pb(II), Cd (II), Sr(II)) during the COVID-19 pandemic

Lujian Lin [a], Bo Yuan [a], Binghuang Zhang [a], Hanyi Li [a], Ran Liao [c], Hualong Hong [a,*], Haoliang Lu [a], Jingchun Liu [a], Chongling Yan [a,b,*]

[a] Key Laboratory of the Ministry of Education for Coastal and Wetland Ecosystems, Xiamen University, Xiamen 361102, PR China
[b] State Key Laboratory of Marine Environmental Science, Xiamen University, Xiamen 361102, PR China
[c] Guangdong Research Center of Polarization Imaging and Measurement Engineering Technology, Shenzhen International Graduate School, Tsinghua University, Shenzhen 518055, PR China

ARTICLE INFO

Keywords:
COVID-19
Disposable face masks
Metals
Adsorption mechanisms
UV radiation

ABSTRACT

The demand for disposable face masks (DFMs) increased sharply in response to the COVID-19 pandemic. However, information regarding the underlying roles of the largely discarded DFMs in the environment is extremely lacking. This study focused on the pristine and UV-aged DFMs as vectors of metal ions (Pb(II), Cd(II), and Sr(II)). Further, the aging mechanism of DFMs with UV radiation as well as the interaction mechanisms between DFMs and metal ions were investigated. Results revealed that the aging process would help to promote more metal ions adsorbed onto DFMs, which was mainly attributed to the presence of oxygen-containing groups on the aged DFMs. The adsorption affinity of pristine and aged DFMs for the metal ions followed Pb(II) > Cd(II) > Sr(II), which was positively corrected with the electronegativity of the metals. Interestingly, we found that even if DFMs were not disrupted, DFMs had similar or even higher adsorption affinity for metals compared with other existing microplastics. Besides, regarding environmental factors, including salinity and solution pH played a crucial role in the adsorption processes, with greater adsorption capacities for pristine and aged DFMs at higher pH values and low salinity. Fourier transform infrared spectroscopy, X-ray photoelectron spectroscopy, and density functional theory further confirmed that the pristine DFMs interacted with the metals mainly through electrostatic interaction, while electrostatic interaction and surface complexation jointly regulated the adsorption of the metals onto aged DFMs. Overall, these findings would help to evaluate environmental behaviors and risks of DFMs associated with metals.

1. Introduction

Since the COVID-19 pandemic, there has been an unprecedented increase in single-use plastics such as gloves, protective medical suits, face masks, takeaway plastics, and medical testing kits [1]. Disposable face masks (DFMs) can effectively prevent respiratory droplets from entering through the mouth and nose, and prevent the discharge of mucosal saliva droplets by the infected [2,3]. In response, people around the world are urged to wear DFMs in public places for the pandemic prevention and control [4]. Generally, DFMs are mainly made of polymer materials such as polypropylene (PP), polyethylene glycol terephthalate (PET) and polystyrene (PE), and consist of four parts: inner layer (fiber material or non-woven), middle layer (melt-blown filter), outer layer (non-woven), and ear ribbon (fiber material) [5,6]. Besides, three kinds of DFMs are widely used by medical personnel and the public, namely surgical or medical masks, respirator masks (N95, FFP2), and non-certified masks (cloth masks) [7,8]. Recently, several high-performance multifunctional DFMs (e.g., biofilm filter, antibacterial, and antiviral) have been developed for better epidemic prevention and control [9]. These multifunctional DFMs are achieved by embedding one or more multifunctional structures into traditional DFMs, for instance, this functional improvement is applied to the synthesis of antimicrobial drug-bonded meltblown filter [9,10].

However, the environmental impact of COVID-19 remains largely underestimated due to the top priority given to air and space prevention of the outbreak and close monitoring of economic and social impacts [11]. According to the World Wide Fund for Nature (WWF), improper disposal of DFMs even at 1% of all masks used can generate

* Corresponding authors.
E-mail addresses: honghl@xmu.edu.cn (H. Hong), ycl@xmu.edu.cn (C. Yan).

https://doi.org/10.1016/j.cej.2022.135613
Received 19 January 2022; Received in revised form 28 February 2022; Accepted 2 March 2022
Available online 5 March 2022

approximately 10 million DFMs per month being dispersed in the environment [12]. These abandoned DFMs can become channels and sources of pathogens and contaminants in the environment [5,13]. For example, some additives in DFMs, e.g., synthetic phenolic, organophosphate antioxidants, and heavy metals (Pb, Cd, and Sb), can be released into the aquatic environment [14–16]. Recent studies have also demonstrated that DFMs could release hundreds of microplastics/nanofibers and up to 10^8 fibers into the environment [6,17,18], which caused a series of negative effects on the ecosystem [7,19,20]. In this regard, thermal treatment methods can effectively treat DFMs waste, and DFMs are used as nitrogen-doped carbon sorbents by thermal carbonization, which can effectively remove Cr(VI) [21,22]. Notably, DFMs can adsorb and release some contaminants (e.g., dyes, antibiotics, U-232, and Ra-226), which potentially enhances the widespread of those contaminants [13,23,24]. However, limited information is known about the interaction behaviors of DFMs with metals. Thus, further investigation is required to fully understand the potential role of DFMs as metals carriers, which will help to assess the environmental risks of DFMs.

In this study, three typical divalent metal ions including lead ions (Pb (II)), cadmium ions (Cd(II)), and strontium ions (Sr(II)) are selected as target pollutants. Pb and Cd are widespread heavy metals in the environment and can be discharged into the aquatic environment through a variety of channels, such as industrial effluents, agriculture wastes, and the application of metal-based coatings in the fishery [25–27]. As for another metal, ^{90}Sr ($T_{1/2}$ = 28.7 years) derived from nuclear power plants, is a classic radioactive metal that can cause persistent chemical and radiological damage to organisms in the environment [28,29]. Notably, Sr ions have high mobility, which makes them one of the essential metal contaminants in the aqueous environment [30].

The aim of this study was to investigate the effects of DFMs properties (e.g., pristine, and UV-aged DFMs) and environmental factors (e.g., solution pH and salinity) on the adsorption of Pb(II), Cd(II), and Sr(II) ions onto DFMs. Further, the aging mechanism of DFMs with UV radiation and the interaction mechanisms between DFMs and the metal ions were elucidated based on the experimental phenomena, characterization analysis as well as quantum chemical methods. Overall, our main purpose was to reveal the potential role of DFMs as a carrier of metal ions in the environment.

2. Materials and methods

2.1. Materials and chemicals

The DFMs used in this study were obtained from a Chinese e-commerce platform (JD. COM). Details of the DFMs include brand (WELLDAY), Size (175 × 95 mm), color (Blue/White), executive standard (YY/T 0969–2013), materials (PP/PET), and weight (3.1228 ~ 3.2665 g). Plastics used for characterization include commercial PP and PET (purity: greater than 99%, size: 200 meshes) were obtained from Zhongcheng Plastic Chemical Co., Ltd (Guangdong, China).

Lead nitrate ($Pb(NO_3)_2$, 99.999%), cadmium nitrate ($Cd(NO_3)_2{\cdot}4H_2O$, 99.999%), and strontium nitrate ($Sr(NO_3)_2$, 99.97%) were purchased from Shanghai Aladdin Bio-Chem Technology Co. Ltd, China. All the other chemicals used (e.g., sodium chloride (NaCl), nitric acid (HNO_3), sodium hydroxide (NaOH)) were analytical grade or higher purity.

2.2. DFMs aging experiment

For UV irradiation, the DFMs were carried out in an aging chamber by six 8 W-UVA lamps (Philips, TL8WBL) with the characteristic wavelengths at 350–400 nm as the light source according to the method of Kyung et al. with minor modifications (Fig. S1) [31]. Specifically, the DFMs were changed in the aging chamber every 24 h on their exposed surface for a period of 14 days. The exposure temperature was maintained at 25 ± 1℃ by circulating cooling air inside the aging chamber through a fan attached to the outside of the system.

2.3. Experimental procedures

Prior to the batch experiments, all glass bottles used were soaked in 5% HNO_3 for 24 h to eliminate metal pollutants on the glass wall, then cleaned with ultrapure water and dried in an oven at 60℃ for 12 h. The stock solutions of Pb(II), Cd(II), and Sr(II) (100 mg/L) were prepared in 1% HNO_3 by dissolving a known quantity of $Pb(NO_3)_2$, $Cd(NO_3)_2{\cdot}4H_2O$, and $Sr(NO_3)_2$, respectively. The adsorption experiments were carried out in 250 mL glass reagent bottle with a lid. A whole DFM and 200 mL sample solutions containing different metal concentrations, 0.01 mol/L $NaNO_3$ (to maintain stable ionic strength), and 0.02% NaN_3 (to inhibit microbial activity) were put into the bottle [32,33]. Next, the bottles were conducted at 25 ℃ and 150 rpm by an oscillator. All samples were performed in triplicates and blank experiments (DFM free) were conducted at the same time.

2.3.1. Adsorption kinetics and isotherms

To obtain the equilibrium time for metal ions adsorption, we first conducted a pre-adsorption experiment with a period of 7 days. As seen in Fig. S2, the Pb(II), Cd(II), and Sr(II) ions adsorption onto the DFMs reached equilibrium almost within 2 days. Therefore, the equilibration time for subsequent adsorption experiments was set to 48 h. Besides, control of pH during adsorption was performed to avoid an increase of solution pH to prevent metal precipitation (Fig. S3).

The kinetics experiments were designed as follows: the initial concentration of metal ions was 5 mg/L; solution pH was 6; and the solution was collected at given time intervals (0.5, 1, 2, 4, 6, 12, 24, 36, 48, 60, and 72 h). The isothermal experiments were performed include: the initial concentrations of metal ions were 1, 3, 5, 10, 20, 30, 50 mg/L; and solution pH was 6.

2.3.2. Effects of salinity and solution pH on the adsorption process

The concentration of NaCl was set (0%, 0.05%, 0.1%, 0.5%, 1%, 2%, and 3.5%) based on the gradient of ionic strength in the fresh-to-seawater systems [34]. Since Pb and Cd solutions will form hydroxide precipitates ($Pb(OH)_2$ and $Cd(OH)_2$) when the solution pH was greater than 8, the solution pH was adjusted to 2, 3, 4, 5, 6, 7, and 8 according to the speciation distributions of Pb, Cd, and Sr (Fig. S3). All other conditions were the same as those used in kinetic experiments.

2.4. Analytical methods and characterization

The Pb(II), Cd(II), and Sr(II) concentrations were detected by inductively coupled plasma optical emission spectrometer (ICP-OES, SPECTROBLUE FMX36, Germany).

Fourier transform infrared spectroscopy with attenuated total reflection equipment (ATR-FTIR), X-ray photoelectron spectroscopy (XPS), and scanning electron microscope equipped with energy dispersive X-ray analysis (SEM-EDX) were conducted to characterize DFMs with and without metal ions adsorbed. The point of zero charge (pH_{zpc}) of the DFM was determined according to the previous protocol [35]. Detailed information about instruments used and the method of pH_{zpc} determined was provided in Supplementary Information.

2.5. Mathematical models and data analysis

In this study, the pseudo first-order model (PFO), pseudo second-order model (PSO), and Elovich models were fitted to adsorption kinetics data. Langmuir and Freundlich models were used to analyze adsorption isotherms. The details of these models are shown in Table S1 of Supplementary Information. All data were analyzed by OriginPro 2020. Density Functional Theory (DFT) B3LYP/def2-TZVP functional was used to optimize the molecular structure, minimize molecular

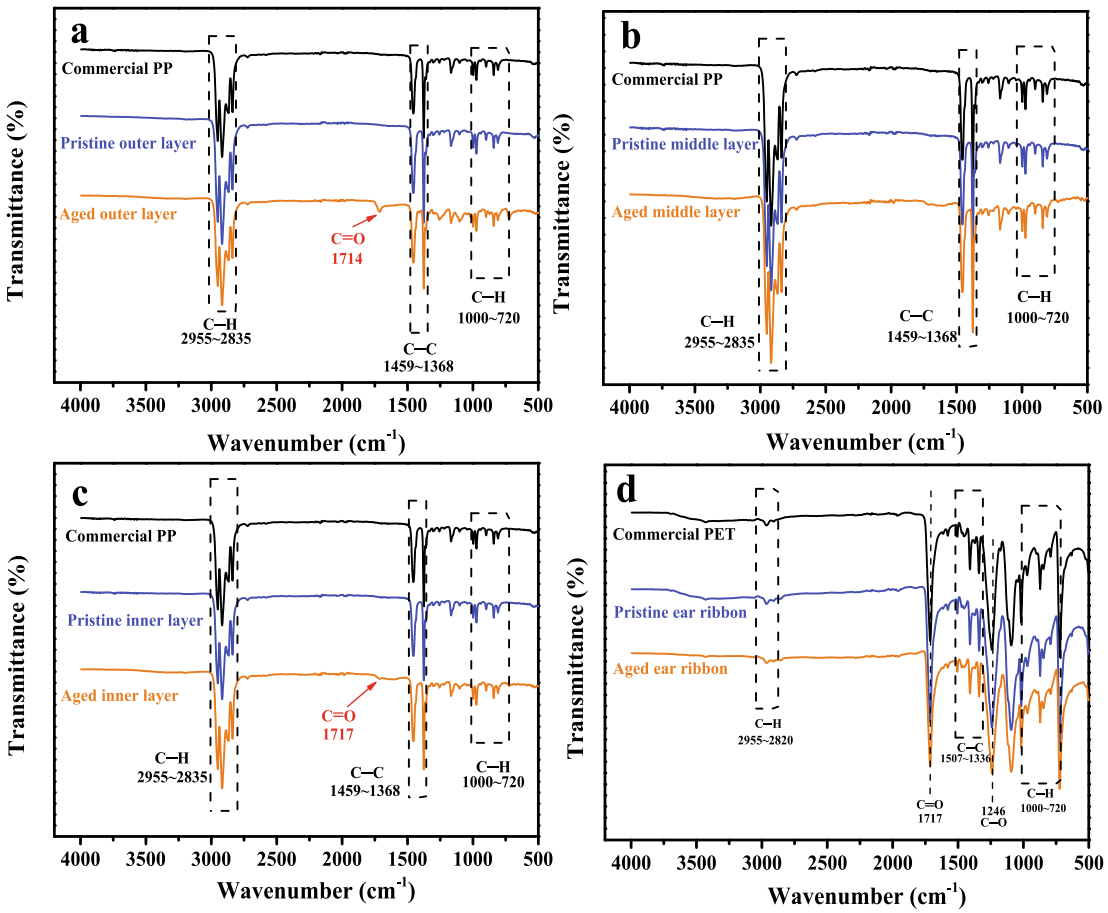

Fig. 1. FTIR spectra of the outer layer (a), middle layer (b), inner layer (c), and ear ribbon (d) of pristine and aged DFMs as well as commercial PP and PET.

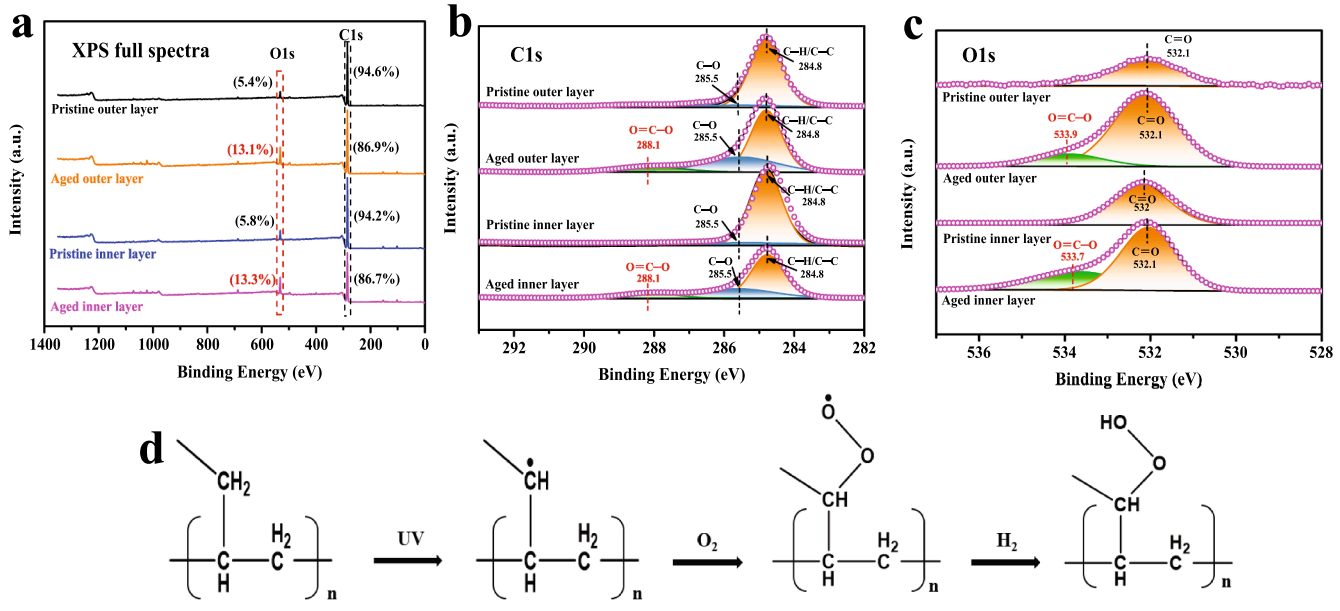

Fig. 2. XPS spectra of full (a), C1s (b), O1s (c) of pristine and aged DFMs; Aging mechanism of DFMs under UV radiation (d).

energy, and calculate the charge distribution and surface electrostatic potential by GaussView 5.0 and Gaussian 16.

The amounts of metal ions adsorbed onto DFMs were calculated according to Eq. (1):.

$$Q_t = \frac{V(C_0 - C_t)}{m} \quad (1)$$

in which Q_t(μg/g) and C_t(μg/L) are the adsorption capacities and

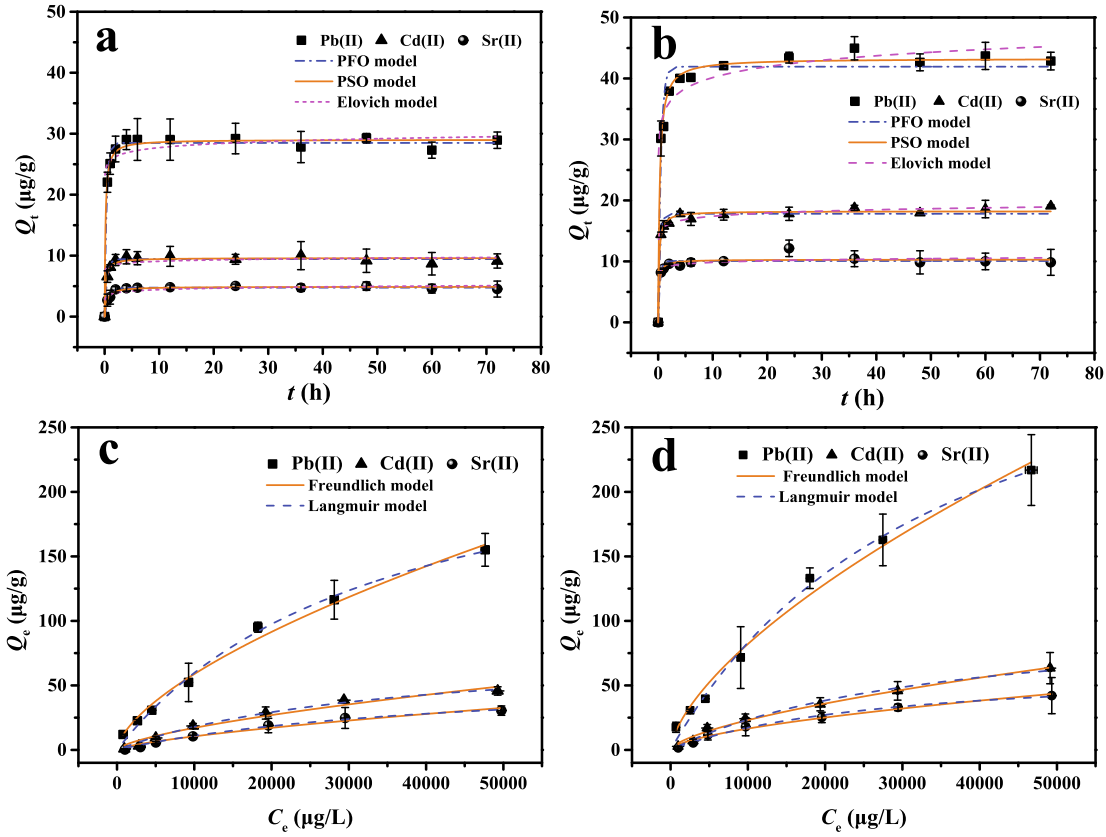

Fig. 3. Adsorption kinetics (a,b) and isotherms (c,d) of the metal ions onto pristine (left column) and aged DFMs (right column).

concentrations of adsorbates at time *t*, respectively; C_0(μg/L) is the initial concentration of metal ions; *m* (g) is the weight of DFMs, and *V* (L) represents the volume of metal ions solution. When the sorption reaches equilibrium, $C_e = C_t$, $Q_e = Q_t$, where C_e(μg/L) and Q_e(μg/g) are the metal ions concentration and adsorption capacities at equilibrium, respectively.

3. Results and discussion

3.1. Aging alters the physical and chemical properties of DFMs

The photodegradation of polymer is mainly initiated by UV radiation, and several reactive oxygen species (ROS) including superoxide radical ($O_2^{\bullet-}$) and hydroxyl radical (•OH) are the primary driving force of the aging processes [36,37]. Here SEM, ATR-FTIR, and XPS were conducted to analyze the changes in the physical and chemical properties of the surface of DFMs during the aging process. It can be seen from SEM that DFMs are composed of many columnar microfibers crossing each other, which is equivalent to the film layer of microplastics aggregate (Fig. S4). As DFMs are exposed to UV radiation, the surface of aged DFMs becomes relatively rough, which may increase the potential adsorption sites of aged DFMs as pollutant carriers. By comparing the FTIR spectra of commercial plastics and DFMs, the outer, middle, and inner layers of DFMs are identified as PP, while the ear ribbon of DFMs is identified as PET (Fig. 1). The result was supported by Ma et al., who quantified and characterized DFMs released microparticles [20]. Interestingly, the new peaks that appeared at 1714 and 1717 cm^{-1} of the outer layer and inner layer of aged DFMs are caused by the C = O stretching vibration of the carboxyl group [38], which is attributed to the surface oxidation of DFMs during the aging process. However, no new chemical bonds are formed in the middle layer and ear ribbon of aged DFMs, indicating that the outer layer and inner layer of DFMs are oxidized first during the aging process. Further, the XPS full spectra show that the atomic content of O1s of the out and inner layers of DFMs increases from 5.37% and 5.78% to 13.11% and 13.34% with the aging of DFMs, respectively (Fig. 2 a). Besides, the growth of O-C = O groups is also observed on aged DFMs by high-resolution XPS spectra of C1s and O1s regions (Fig. 2 b & c). These results are basically consistent with the FTIR analysis. Generally, photoinitiators can be classified as bond a-cleavage type (Norrish type I) or hydrogen abstraction type (Norrish type II) [39]. The appearance of –COOH groups on the surface of aged DFMs may be due to the UV-induced breakage of the C–H bond and subsequent reaction with oxygen to form peroxy radicals (ROO•), further ROO• can absorb hydrogen atoms from the air, thereby forming hydroperoxide groups (RCOOH) (Fig. 2 d) [40]. Therefore, this aging process can be well explained by Norrish type II photoreaction. A similar result was reported by Liu et al., who studied that UV radiation aggravated the aging process of microplastics [41]. Tang et al. also found that carboxyl functional groups newly appeared on the surface of naturally aged nylon plastics compared to the pristine nylon plastics [42].

3.2. Interface behavior between metal ions and DFMs

3.2.1. Adsorption kinetics

The plots of fitting by PFO, PSO, and Elovich models for Pb(II), Cd (II), and Sr(II) ions adsorption onto pristine and aged DFMs are presented in Fig. 3 (a & b), and the relevant fitting parameters are provided in Table S2. In general, the PFO model assumes that the adsorption of metal ions is one site binding mechanism [43], while the PSO and Elovich models assume that the adsorption process is predominated by chemical force [44]. The excellence of consensus between experimental data the model-predicted values is represented by adjusted R^2 and chi square (χ^2). As summarized in Table S2, the values of relatively high adjusted R^2 with low χ^2 suggest that the adsorption processes of Pb(II), Cd(II), and Sr(II) ions onto pristine are best fitted to PFO model, while aged DFMs conform to PSO and Elovich models. The results indicate that

Table 1
Parameters of the isotherm models for the adsorption of the metal ions onto the pristine and aged DFMs.

DFMs	Metals	Parameters Freundlich model K_F ($(\mu g \cdot g^{-1})/(\mu g \cdot L^{-1})^{1/n}$)	n_F	Adj.R^2	χ^2	Langmuir model K_L (L/μg)	Q_m (μg/g)	Adj.R^2	χ^2
Pristine	Pb(II)	0.165	1.57	0.990	28.9	2.90×10^{-5}	265.63	0.994	17.1
	Cd(II)	0.039	1.51	0.960	12.4	2.89×10^{-5}	79.75	0.989	3.45
	Sr(II)	0.016	1.42	0.966	4.71	2.30×10^{-5}	58.54	0.990	1.36
Aged	Pb(II)	0.209	1.54	0.988	71.2	2.76×10^{-5}	384.16	0.993	42.5
	Cd(II)	0.064	1.56	0.984	5.45	2.86×10^{-5}	105.32	0.986	5.07
	Sr(II)	0.062	1.65	0.982	3.86	3.65×10^{-5}	64.34	0.992	1.83

Table 2
Comparison of Q_m (μg/g) obtain from Langmuir model between the results of this work and others found in the literatures.

Metals	Types of plastics	pH	size	Temperature (℃)	Q_m (μg/g)	References
Pb(II)	Pristine DFM	6.0	175 × 95 mm[a]	25	265.63	This work
	Aged DFM	6.0	175 × 95 mm[a]	25	384.16	
	Pristine PS	NM[b]	0.1 μm	25 ± 2	160.00	[40]
	Aged PS	NM[b]	0.1 μm	25 ± 2	202.00	
	Pristine PVC	6.5	280 μm	25	2518 ± 125	[49]
	Beached PE	NM[b]	NM[b]	20 ± 1	0.72	[67]
	Pristine PE	6.5	~ 4 mm	25	0.19	[68]
	Beached PE	6.5	~ 4 mm	25	2.74	
	Pristine PET	6.3	< 5 mm	NM[b]	4930.00	[69]
	Pristine PP	6.3	< 5 mm	NM[b]	5550.00	
Cd(II)	Pristine DFM	6.0	175 × 95 mm[a]	25	79.75	This work
	Aged DFM	6.0	175 × 95 mm[a]	25	105.32	
	Pristine PS	NM[b]	0.1 μm	25 ± 2	105.00	[40]
	Aged PS	NM[b]	0.1 μm	25 ± 2	175.00	
	Pristine PS	4.0	NM[b]	25	20.15	[70]
	Pristine PP	NM[b]	74 μm	25	36.10	[71]
	Pristine PVC	6.5	280 μm	25	1748 ± 505	[49]
	Beached PE	NM[b]	NM[b]	20 ± 1	0.01	[67]
	Pristine PE	6.5	~ 4 mm	25	0.01	[68]
	Beached PE	6.5	~ 4 mm	25	0.25	
	Pristine PET	6.0	75 μm	24 ± 1	250 ± 10	[27]
	Pristine PVC	6.5	280 μm	25	1748 ± 505	[49]
Sr(II)	Pristine DFM	6.0	175 × 95 mm[a]	25	58.54	This work
	Aged DFM	6.0	175 × 95 mm[a]	25	64.34	
	Pristine PP	NM[b]	100–150 mm	25	68 ± 12.6	[72]
	Pristine PET	NM[b]	100–150 mm	25	360 ± 79.2	[29]
	Pristine PE	NM[b]	100–150 mm	25	470 ± 106	
	Pristine PVC	NM[b]	100–150 mm	25	790 ± 238	

Note: 175 × 95 mm[a] (A whole DFM); NM[b] (Not Mentioned); Abbreviations: PP (Polypropylene); PET (Polypropylene Terephthalate); PS (Polystyrene); PVC (Polyvinyl Chloride); PE (Polyethylene).

the metal ions adsorption onto pristine and aged DFMs is mainly dependent on the physisorption and chemical interaction, respectively [45]. We found that the new oxygen-containing functional group (–COOH) appeared on the surface of aged DFMs in the above discussion, which may be an important reason for this result. In addition, the equilibrium adsorption capacities for pristine DFMs ($Q_{e,1}$) and aged DFMs ($Q_{e,2}$) obtained from PFO and PSO models, which follows Pb(II) (28.49 μg/g) > Cd(II) (9.44 μg/g) > Sr(II) (4.76 μg/g) and Pb(II) (43.27 μg/g) > Cd(II) (18.23 μg/g) > Sr(II) (10.30 μg/g), respectively. Obviously, the adsorption capacity of aged DFMs is higher than those of pristine DFMs. A similar observation has been reported by Mao et al., who studied that the adsorption capacity of PS microplastics for Pb(II) and Cd(II) was closely attributed to their aging degree [40]. Different adsorption capacities of DFMs for Pb(II), Cd(II), and Sr(II) ions may be related to the intrinsic properties of different metal ions [46]. If electrostatic interaction is the key adsorption mechanism between DFMs and these divalent metal ions, the adsorption affinity will be positively correlated with the electronegativity of metal ions. As expected, the Pauling electronegativity order of the three metals is Pb (2.33) > Cd (1.69) > Sr (0.95) [47,48], which indicates that electrostatic interaction plays an important role in the metals adsorption onto pristine and aged DFMs. This was supported by Pan et al., who found that the adsorption capacities for biogas residue-based adsorbent were in order of Pb > Cu > Fe > Cd > Zn, which was linear with the electronegativity of these metal ions [48]. Zou et al. also reported that microplastics exhibited relatively stronger adsorption capacity for Pb(II) than those for Cu(II) and Cd(II) due to the strong electrostatic attraction [49]. Besides, Yang et al. observed that the sequence of maximum adsorption amount was Pb (II) > Ni(II) > Sr(II) onto graphene oxides [50]. Overall, the results from adsorption kinetics imply that the aging process of DFMs will help to promote more metal ions to appear on the surface of aged DFMs than those of pristine DFMs, and electronegativity of the metal ions can be used as an indicator parameter to the adsorption affinity between the DFMs and the metal ions.

3.2.2. Adsorption isotherms

The adsorption isotherms of Pb(II), Cd(II), and Sr(II) ions onto pristine and aged DFMs are shown in Fig. 3 (c & d). Freundlich and Langmuir models are used to analyze the adsorption process for pristine and aged DFMs, and the fitting parameters are listed in Table 1. Comparing the adjusted R^2 and χ^2 values of Freundlich and Langmuir models, the metal ions adsorption processes onto both the pristine and aged DFMs are well described by Langmuir model. This result indicates that the metal ions adsorbed onto both the pristine and aged DFMs may be

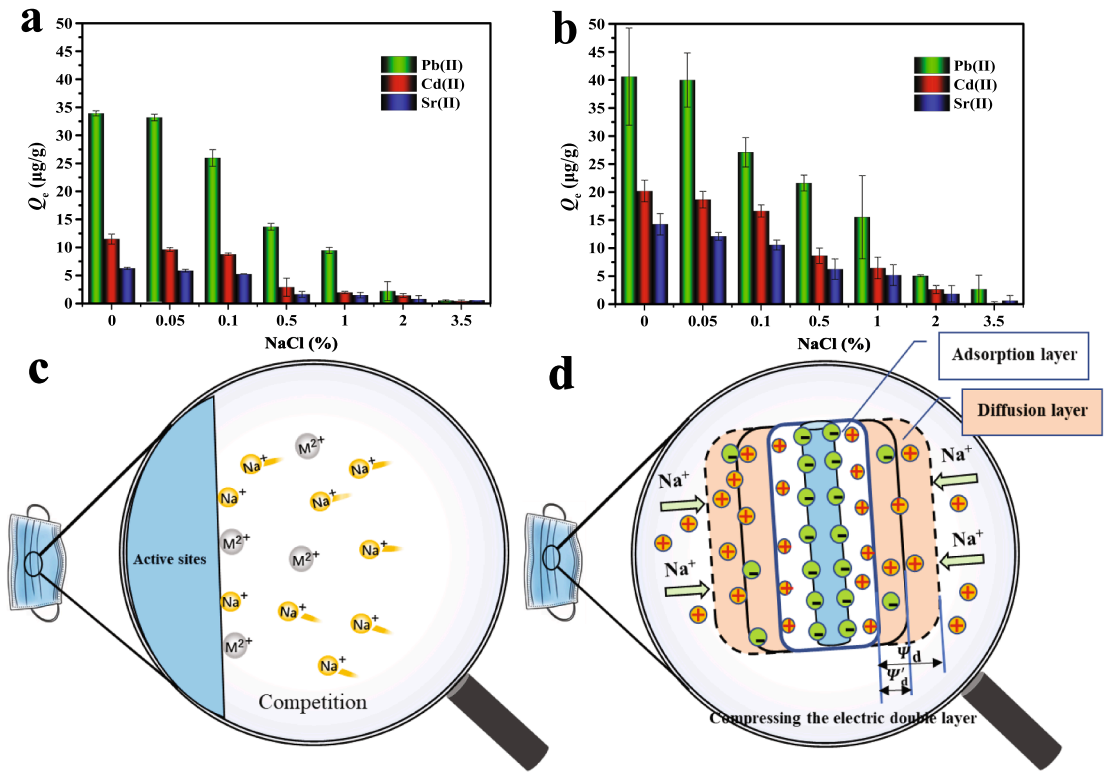

Fig. 4. Influence of the NaCl on the adsorption of metal ions (Pb(II), Cd(II), and Sr(II)) onto pristine (a) and aged (b) DFMs; Schematic illustrating the competition of the active sites (c) and the compression of the electric double layer thickness of the DFMs surfaces (d) is due to the addition of a large amount of Na^+.

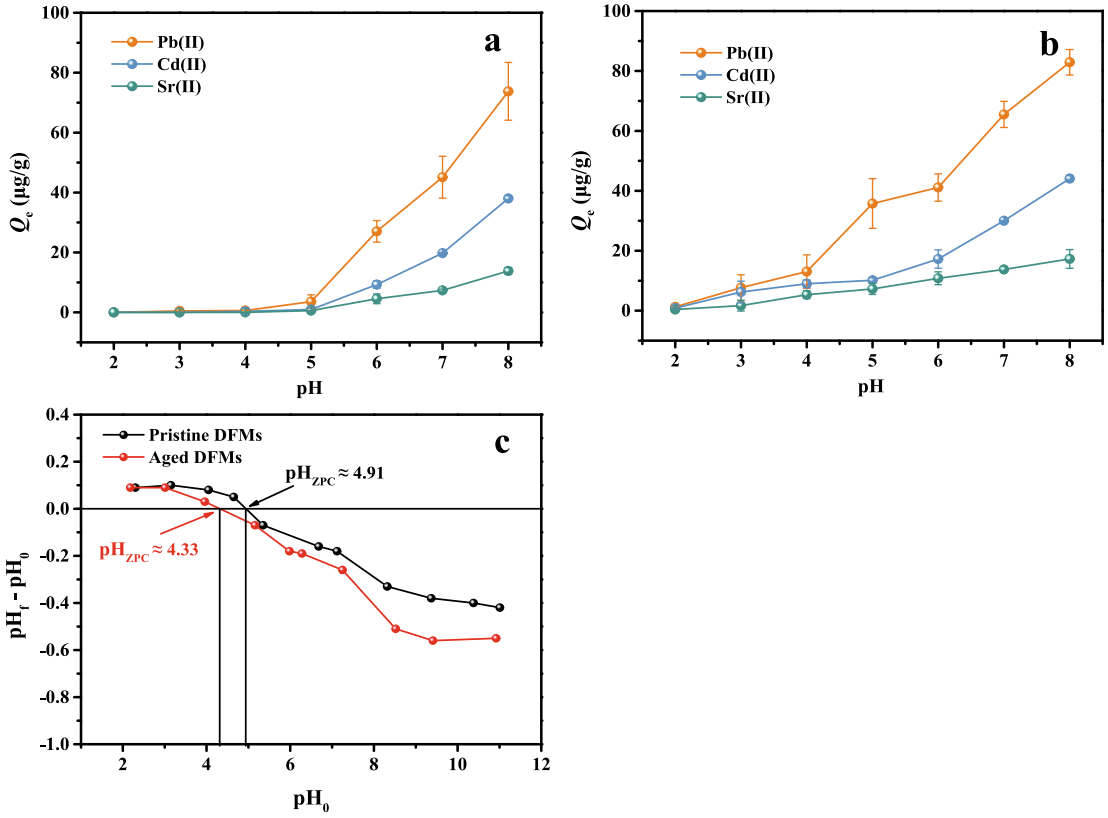

Fig. 5. Influence of solution pH on the adsorption of metal ions (Pb(II), Cd(II), and Sr(II)) onto pristine (a) and aged (b) DFMs; Net surface charge of pristine and aged DFMs as a function of initial solution pH (c).

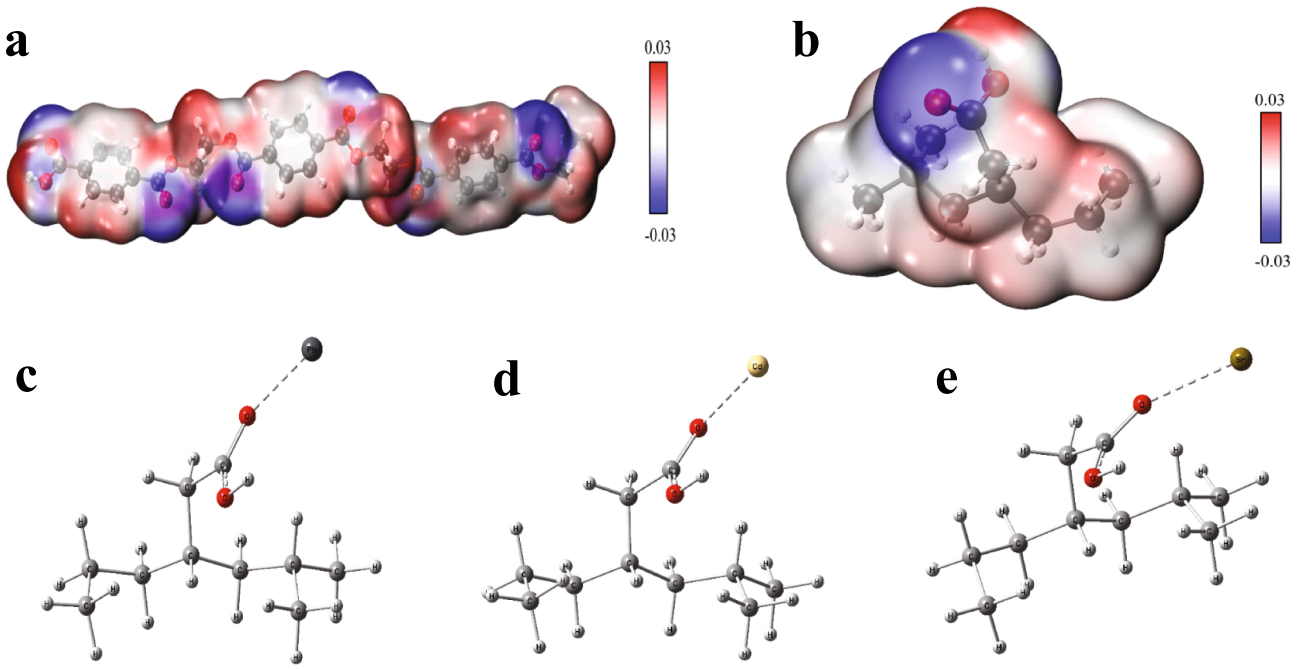

Fig. 6. The surface electrostatic potential of the optimized geometry of PET (n = 3) (a) and the most stable structure of PP (n = 3) with –COOH group (b) obtained at the B3LYP/def2-TZVP level; The optimized complexes between the most stable structure of PP (n = 3) with –COOH group and different cations including Pb^{2+} (c), Cd^{2+} (d), and Sr^{2+} (e).

monolayer adsorption and homogeneous surfaces [51]. For Langmuir model, the Q_m of pristine and aged DFMs follows the order: Pb(II) (265.63 μg/g) > Cd(II) (79.75 μg/g) > Sr(II) (58.54 μg/g) and Pb(II) (384.16 μg/g) > Cd(II) (105.32 μg/g) > Sr(II) (64.34 μg/g), respectively. As the same kinetic analysis above, the pristine and aged DFMs present a higher adsorption affinity for Pb(II), followed by Cd(II) and Sr(II). Meanwhile, these metal ions prefer to adsorb onto the aged DFMs surface compared to the pristine DFMs. In our previous studies, we found that even if DFMs are not disrupted, DFMs have similar or even higher adsorption affinity for antibiotics compared with other existing microplastics [23]. Therefore, here we summarize Q_m values of metal ions adsorbed onto microplastics reported from the previous paper (Table 2). Notably, the adsorption capacities of DFMs for the metal ions are higher than those of several microplastics, which emphasizes the non-negligible role of DFMs as the metal ions carriers in the environment. Thus, further attention should be paid to the risks associated with the extensive use of DFMs in water environments, and relevant environmental management norms should be urgently and properly formulated.

3.3. Effects of environmental factors

3.3.1. Salinity

The effects of NaCl as a background salinity on Pb(II), Cd(II), and Sr (II) adsorption by the pristine and aged DFMs are illustrated in Fig. 4 (a & b). It is found that Pb(II), Cd(II), and Sr(II) adsorption onto both the pristine and aged DFMs decreases for increasing NaCl concentration. That the extent of metal ions adsorption is sensitive to changes in the content of salinity, indicating that the adsorption capacities of DFMs for metal ions in low-salinity environments (e.g., rivers and lakes) is stronger than those in high-salinity environments (e.g., oceans). Similar results have been reported in studies of microplastics and metal ions. For example, Holmes et al. studied the adsorption of Cd, Co, Cr, Cu, Ni, and Pb onto virgin and beached microplastics under the different salinity environments, and concluded that the increase of salinity inhibited the adsorption behavior of microplastics to these metal ions [52]. Zou et al. also highlighted that the adsorption of Cd, Cu, and Pb by microplastics could be affected by salinity [49]. For this phenomenon, several reasons mainly including i) Na^+ favors competition with Pb(II), Cd(II), and Sr(II) for adsorption sites by its smaller hydrated ionic radius (Fig. 4 c) [53]; ii) the electrical double layer of the DFMs surface is compressed by the addition of Na^+ (Fig. 4 d) [54]. Herein, the main inhibition effect of Na^+ can be described by the total free energy change of adsorption (ΔG_{adso}), which is related to the electrostatic free energy change (ΔG_{elect}) as follows (2) [55]:.

$$\Delta G_{elect} = ZF\Psi_d \quad (2)$$

in which Z, F, Ψ_d are the ionic charge, the Faraday constant (96487C), and the potential in the plane of the metal ions, respectively. The electrostatic potential decreased ($\Psi_d \rightarrow \Psi_d'$) with the increase of Na^+, which results in the coulombic energy decreased [55]. Therefore, NaCl content significantly inhibits the adsorption capacities of DFMs for metal ions. Furthermore, these results also indicate that the adsorption processes may be predominated by electrostatic interaction and/or surface complexation [44,54]. A similar result was reported by Qi et al., who reported that the NaCl reduced Pb(II) adsorption amount onto microplastics was contributed to electrostatic attraction and chemical adsorption [25]. Tang et al. also observed that NaCl could weaken the electrostatic attraction between nylon microplastics and metal ions (Cu, Zn, and Ni), whereas the surface complexation between Na^+ and carboxyl groups of microplastics was also an important factor [42].

3.3.2. Solution pH

Generally, most natural water has a pH range of 5 to 9 [42]. However, Pb and Cd solutions will form hydroxide precipitates ($Pb(OH)_2$ and $Cd(OH)_2$) when the solution pH is greater than 8 (Fig. S3), thus the solution pH is only set within the range of 8. It is observed that the adsorption of Pb(II), Cd(II), and Sr(II) ions onto both the pristine and aged DFMs is significantly pH-dependent, with greater adsorption capacities for pristine and aged DFMs at higher pH values (Fig. 5 a & b). The pH_{zpc} of pristine and aged DFMs is determined to be 4.91 and 4.33, respectively (Fig. 5 c). At solution pH > pH_{zpc}, negative charge sites are mainly distributed on the surface of DFMs, which is beneficial to the metal ions adsorption. Interestingly, the metal ions adsorption

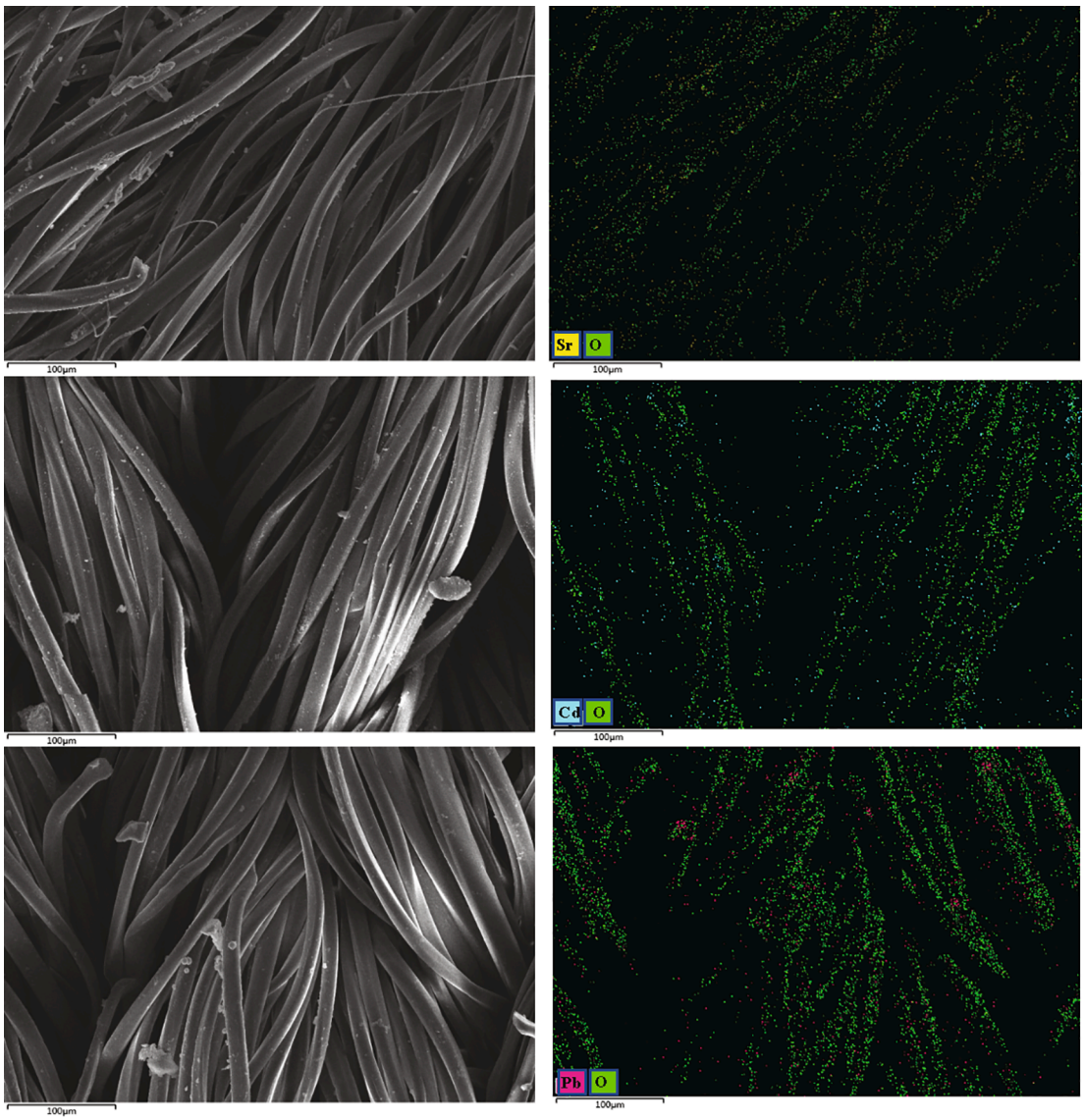

Fig. 7. SEM-EDX mapping images of DFMs after Pb(II), Cd(II), and Sr(II) adsorption.

capacities onto pristine DFMs are negligible at pH 2, 3, and 4. This phenomenon indicates that the adsorption process for pristine DFMs is predominated by electrostatic interaction. However, the metal ions can still be adsorbed onto aged DFMs at lower pH values, which implies that the adsorption process for aged DFMs is not only controlled by electrostatic interaction, but chemisorption may also be present in the process. This was supported by Zou et al., who that the Pb(II), Cd(II), and Cu(II) adsorption onto PE and PVC microplastics were predominated by electrostatic interaction and surface complexation [49]. Fu et al. also reported that electrostatic interaction and surface complexation were main interaction mechanisms between aged PE microplastics and Pb(II) [56].

3.4. Adsorption mechanisms

We propose that the adsorption processes of the three metal ions onto pristine and aged DFMs mainly involve electrostatic interaction and surface complexation according to the above phenomena. To further demonstrate the interaction mechanisms between DFMs and the metal ions, some characterization including FTIR, SEM-mapping, XPS as well as quantum chemistry methods were performed.

It can be seen from the FTIR spectra that no new peaks appeared or disappeared in pristine DFMs after the metal ions adsorption (Fig. S5), which indicates that the adsorption process of pristine DFMs is predominated by physical force [57]. However, the absorption peak of C = O in the outer and inner layers of aged DFMs disappeared (Fig. S5), suggesting that Pb(II), Cd(II), and Sr(II) ions bind aged DFMs likely through $–COO^-$ groups [55].

Furthermore, XPS spectra were conducted to synergistically confirm the results of FTIR analysis. The additional Pb4f, Cd3d, and Sr3d peaks are observed in XPS full spectra after the metal ions adsorption, which confirms that Pb(II), Cd(II), and Sr(II) ions are indeed adsorbed onto aged DFMs (Fig. S6 a). The O1s high-resolution spectra of aged DFMs (outer layer) after Pb(II), Cd(II), and Sr(II) ions adsorption are displayed in Fig. S6 (b). It can be observed that the Pb-O (531.3 eV) and Cd-O (531.7 eV) appeared in the O1s high-resolution spectra, which indicates that Pb and Cd are adsorbed to the surface of aged DFMs by O-containing groups. Similar results were also reported by Dong et al., who found that As-O (530.6 eV) peak newly appeared in interaction process between As(III) and polytetrafluoroethylene microplastics [58]. However, no new Sr-O peak appears in aged DFMs after Sr(II) adsorption, which may be related to less adsorption amount [42]. After the metals adsorption, the binding energy of O-C = O increased from 533.9 eV to 534.1, 534.1, and 534.1 eV, respectively, and the related relationship

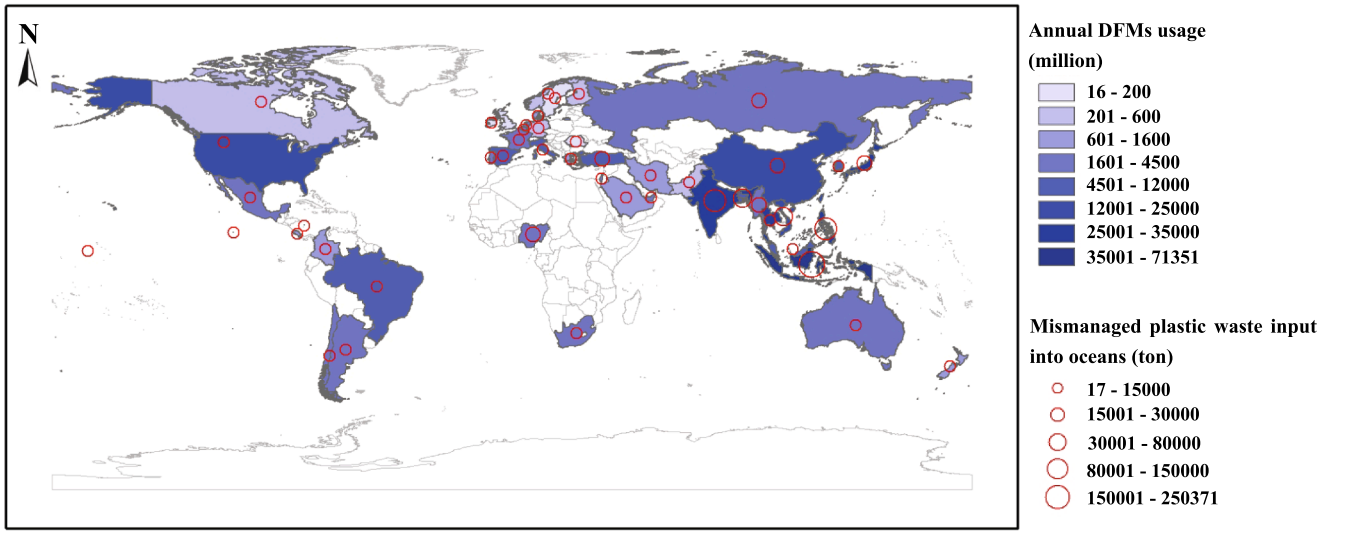

Fig. 8. Annual DFMs usage and annual plastics waste from mismanaged DFMs input into oceans in 46 countries (The data were obtained from Chowdhury et al. and listed in Table S4 [4]; the white parts of the map were the uncounted areas).

between the average oxygen charge (Q) and binding energy (BE) was reported as equation (3) [59]:.

$$Q = -4.372 + \frac{(385.023 - 8.976 \times (545.509 - O1sBE))^{1/2}}{4.488} \quad (3)$$

Herein the increase of Q implies that the electron density of the oxygen atom in –COOH decreased and the dissociation degree of proton increased [42]. This suggests that electrostatic attraction is involved in the adsorption of metals onto aged DFMs. In addition, the –COOH group binds metals as electron donors, which likely suggests that surface complexation plays a crucial role in the adsorption process [60]. Thus, the possible reaction for the divalent metal ions (represented by M^{2+}) adsorption onto aged DFMs surface functional groups can be described as follows [44,61]:.

$$a \equiv DFMs - OOH + bM^{2+} + cH_2O \leftrightarrow (\equiv DFMs - OO)_aM_b(OH)_c^{(2b-a-c)} + (a + c)H^+ \quad (4)$$

where $\equiv DFMs - OOH$ is the surface group in the DFMs phase; $(\equiv DFMs - OO)_aM_b(OH)_c^{(2b-a-c)}$ represent surface complexes; a, b, and c are stoichiometric coefficients.

Based on the surface groups identified by FTIR and XPS analysis, the structures of PET (n = 3) and PP (n = 3) were fully optimized at B3LYP /def2-TZVP level of theory by Gaussian 16. The vibrational frequencies of the optimized structure were carried out at the same level. The structure was characterized as a local energy minimum on the potential energy surface by verifying that all the vibrational frequencies were real. To predict the most possible location of the COOH group in aged DFMs, three different structures were considered and optimized, and their energies were also calculated to compare their relative stability. It is found that the structure (denoted by M) with the COOH group substituted with the H on the CH_3 group is the energy minimum (Table S3). The Visual Molecular Dynamics (VMD) program was used to plot the color-filled was surfaces graphs to visualize the molecular electrostatic potential of PET (n = 3) and M (Fig. 6 a & b). As shown in Fig. 6 (a & b), a few surfaces of PET and M present a negative electrostatic potential, which is related to the oxygen atoms on the surface. This result indicates that the O atom can be the binding site with these metal ions by electrostatic attraction [62]. Besides, SEM-mapping images show that Pb(II), Cd(II), and Sr(II) ions are mainly distributed with O atom, which further confirms this result (Fig. 7). As mentioned above, surface complexation likely exists between aged DFMs and these metal ions, here the complexes formed between M and these metal cations including Pb^{2+}, Cd^{2+}, and Sr^{2+} are optimized and their interaction energies are also calculated at the B3LYP /def2-TZVP level for comparison (Fig. 6 (c, d, & e). The result indicates that the interaction energy of M with Cd^{2+} is strongest (-142.62 kcal/mol) among the three metal cations, followed by Pb^{2+} (-104.87 kcal/mol) and Sr^{2+} (-79.33 kcal/mol). However, the adsorption affinity of the three metal cations onto aged DFMs followed the order of Pb(II) > Cd(II) > Sr(II), which is inconsistent with interaction energy between M and the three metal cations. This suggests that surface complexation is not the only interaction mechanism between aged DFM and the three metal ions. Similar results were also reported by Fu et al. and Zou et al. [49,56].

In summary, oxygen-containing functional groups in pristine and aged DFMs provide binding sites for Pb^{2+}, Cd^{2+}, and Sr^{2+} adsorption. The pristine DFMs interact with the three metal ions mainly through electrostatic interaction, while electrostatic interaction and surface complexation jointly regulate the adsorption of three metal ions onto aged DFMs.

3.5. Environmental implication

The demand for DFMs increased sharply in response to the COVID-19 pandemic. It is assessed that about 289.63 billion DFMs are used per year in Asian countries, while European countries consume 61.02 billion DFMs (Fig. 8). While local and international authorities have developed many policies for the safe disposal of COVID-19 waste, it is challenging for authorities to implement these policies on a large scale. Some countries, such as China, established administrative orders early in the pandemic to ensure the proper recovery of DFMs. However, in many countries, especially in developing and underdeveloped countries (e.g., Indonesia, Philippines, and India), the disposal and regulation of DFMs still are very lacking [4]. It is predicted that more than 2.37 million tons of improperly disposed of DFMs enter the oceans each year (Fig. 8). As expected, the amount of DFMs on rivers and beaches seems to be significantly higher than anywhere else, acting as highways and sinks, respectively [63]. For example, discarded DFMs have been found to be increasingly common on many South American coasts [8]. In Kenya, there are 10 times more DFMs on the beach than on the street [64]. In Jakarta Bay, about 492 DFMs are collected daily from the Cilincing and Marunda Rivers [65]. These DFMs, after reaching the aquatic environment, can adsorb or release some pollutants, posing a potential threat to the biota and ecological functions of habitats in aquatic ecosystems [63].

Herein, our findings reveal that DFMs can act as a carrier of metal ions in the environment. These metals may further affect the ecological safety of the aquatic environment with the release of microplastics or nanofibers from DFMs [17], which possibly poses a great threat not only to the local biota but also to humans' health via the food chain [5]. This study focuses on the interface behaviors and mechanisms between DFMs and metals, we also found some additional environmental effects generated by DFMs (unpublished data). Therefore, we further reveal the neglected environmental impact of DFMs and advocate for strengthening the responsible regulation of DFMs. It is worth noting that other types of masks, such as cloth masks (which are very popular in some countries) consisting of polyester or cotton, etc., may have different environmental impacts than traditional DFMs [66]. In addition, further studies also should be conducted to transfer contaminants and microplastics from biofilm-developed DFMs to environments and organisms to further assess the potential risks of DFMs.

4. Conclusions

In this study, a clear understanding of the aging properties of DFMs under the UV radiation as well as the interaction mechanisms between DFMs and metals were investigated. We found that the aging of DFMs, salinity, solution pH had great effects on Pb(II), Cd(II), and Sr(II) ions adsorption. In general, the aging process would help to promote more metal ions adsorbed onto aged DFMs, which was mainly attributed to the presence of –COOH groups on the surface of aged DFMs. Regarding environmental factors including salinity and pH played a crucial role in the adsorption processes, with greater adsorption capacities for pristine and aged DFMs at higher pH values and low salinity. In addition, the adsorption affinity of pristine and aged DFMs for the metal ions followed Pb(II) > Cd(II) > Sr(II), which was positively corrected with the electronegativity of the metal ions. Interestingly, we found that even if DFMs were not disrupted, DFMs had similar or even higher adsorption affinity for metals compared with other existing microplastics. Overall, the pristine DFMs interacted with the three metal ions mainly through electrostatic interaction, while electrostatic interaction and surface complexation jointly regulated the adsorption of three metal ions onto aged DFMs. These results revealed the underlying roles of the largely discarded DFMs in the environment and highlighted that aging could enhance the role of DFMs in metals migration and fate.

Declaration of Competing Interest

The authors declare that they have no known competing financial interests or personal relationships that could have appeared to influence the work reported in this paper.

Acknowledgments

The authors would like to acknowledge the editor and anonymous reviewers whose comments and advice greatly improved the quality of this paper. We gratefully acknowledge the support of this work by National Important Scientific Research Programme of China (2018YFC1406600) and National Natural Science Foundation of China (31870483, 31530008).

Appendix A. Supplementary data

Supplementary data to this article can be found online at https://doi.org/10.1016/j.cej.2022.135613..

References

[1] N. Parashar, S. Hait, Plastics in the time of COVID-19 pandemic: Protector or polluter? Sci. Total Environ. 759 (2021), 144274 https://doi.org/10.1016/j.scitotenv.2020.144274.

[2] M.H. Chua, W. Cheng, S.S. Goh, J. Kong, B. Li, J.Y.C. Lim, L. Mao, S. Wang, K. Xue, L. Yang, E. Ye, K. Zhang, W.C.D. Cheong, B.H. Tan, Z. Li, B.H. Tan, X.J. Loh, Face Masks in the New COVID-19 Normal: Materials, Testing, and Perspectives, Research. 2020 (2020) 1–40. https://doi.org/10.34133/2020/7286735.

[3] T.E. Stone, W. Kunaviktikul, M. Omura, M. Petrini, Facemasks and the Covid 19 pandemic: What advice should health professionals be giving the general public about the wearing of facemasks? Nurs. Heal. Sci. 22 (2020) 339–342, https://doi.org/10.1111/nhs.12724.

[4] H. Chowdhury, T. Chowdhury, S.M. Sait, Estimating marine plastic pollution from COVID-19 face masks in coastal regions, Mar. Pollut. Bull. 168 (2021), 112419, https://doi.org/10.1016/j.marpolbul.2021.112419.

[5] T.A. Aragaw, Surgical face masks as a potential source for microplastic pollution in the COVID-19 scenario, Mar. Pollut. Bull. 159 (2020), 111517, https://doi.org/10.1016/j.marpolbul.2020.111517.

[6] M. Shen, Z. Zeng, B. Song, H. Yi, T. Hu, Y. Zhang, G. Zeng, R. Xiao, Neglected microplastics pollution in global COVID-19: Disposable surgical masks, Sci. Total Environ. 790 (2021), 148130, https://doi.org/10.1016/j.scitotenv.2021.148130.

[7] S. Dharmaraj, V. Ashokkumar, S. Hariharan, A. Manibharathi, P.L. Show, C. T. Chong, C. Ngamcharussrivichai, The COVID-19 pandemic face mask waste: A blooming threat to the marine environment, Chemosphere. 272 (2021), 129601, https://doi.org/10.1016/j.chemosphere.2021.129601.

[8] M. Ardusso, A.D. Forero-López, N.S. Buzzi, C.V. Spetter, M.D. Fernández-Severini, Science of the Total Environment COVID-19 pandemic repercussions on plastic and antiviral polymeric textile causing pollution on beaches and coasts of South America, Science of The Total Environment 763 (2021) 144365.

[9] V. Babaahmadi, H. Amid, M. Naeimirad, S. Ramakrishna, Biodegradable and multifunctional surgical face masks: A brief review on demands during COVID-19 pandemic, recent developments, and future perspectives, Sci. Total Environ. 798 (2021), 149233, https://doi.org/10.1016/j.scitotenv.2021.149233.

[10] H. Huang, H. Park, Y. Liu, J. Huang, On-Mask Chemical Modulation of Respiratory Droplets, Matter. 3 (2020) 1791–1810, https://doi.org/10.1016/j.matt.2020.10.012.

[11] A.L. Patrício Silva, J.C. Prata, T.R. Walker, A.C. Duarte, W. Ouyang, D. Barcelò, T. Rocha-Santos, Increased plastic pollution due to COVID-19 pandemic: Challenges and recommendations, Chem. Eng. J. 405 (2021), 126683, https://doi.org/10.1016/j.cej.2020.126683.

[12] WWF, 2020. Nello smaltimento di macherine e guanti serve resposabilit'a.https://www. wwf.it/scuole/?53500%2FNello-smaltimento-di-mascherine-eguantiserveresponsabilita– World Wide Fund for Nature. [Accessed on January2021].

[13] I. Anastopoulos, I. Pashalidis, Single-use surgical face masks, as a potential source of microplastics: Do they act as pollutant carriers? J. Mol. Liq. 326 (2021), 115247 https://doi.org/10.1016/j.molliq.2020.115247.

[14] J. Fernández-Arribas, T. Moreno, R. Bartrolí, E. Eljarrat, COVID-19 face masks: A new source of human and environmental exposure to organophosphate esters, Environ. Int. 154 (2021) 106654.

[15] R. Liu, S.A. Mabury, Single-Use Face Masks as a Potential Source of Synthetic Antioxidants to the Environment, Environ. Sci. Technol. Lett. 8 (8) (2021) 651–655.

[16] G.L. Sullivan, J. Delgado-Gallardo, T.M. Watson, S. Sarp, An investigation into the leaching of micro and nano particles and chemical pollutants from disposable face masks - linked to the COVID-19 pandemic, Water Res. 196 (2021), 117033, https://doi.org/10.1016/j.watres.2021.117033.

[17] S. Morgana, B. Casentini, S. Amalfitano, Uncovering the release of micro/nanoplastics from disposable face masks at times of COVID-19, J. Hazard. Mater. 419 (2021), 126507, https://doi.org/10.1016/j.jhazmat.2021.126507.

[18] L. Li, X. Zhao, Z. Li, K. Song, COVID-19: Performance study of microplastic inhalation risk posed by wearing masks, J. Hazard. Mater. 411 (2021) 1–9, https://doi.org/10.1016/j.jhazmat.2020.124955.

[19] J. Il Kwak, Y.J. An, Post COVID-19 pandemic: Biofragmentation and soil ecotoxicological effects of microplastics derived from face masks, J. Hazard. Mater. 416 (2021), 126169, https://doi.org/10.1016/j.jhazmat.2021.126169.

[20] J. Ma, F. Chen, H. Xu, H. Jiang, J. Liu, P. Li, C.C. Chen, K. Pan, Face masks as a source of nanoplastics and microplastics in the environment: Quantification, characterization, and potential for bioaccumulation, Environ. Pollut. 288 (2021), 117748, https://doi.org/10.1016/j.envpol.2021.117748.

[21] L. Ali, M.S. Kuttiyathil, M. Altarawneh, Catalytic upgrading of the polymeric constituents in Covid-19 masks, J. Environ. Chem. Eng. 10 (2022) 106978. https://doi.org/10.1016/j.jece.2021.106978.

[22] A. Bumajdad, M.J.H. Khan, The reuse of disposable COVID-19 surgical masks as a nitrogen-enrichment agent and structure promotor for a wild plant-derived sorbent, J. Ind. Eng. Chem. 102 (2021) 163–176, https://doi.org/10.1016/j.jiec.2021.07.003.

[23] L. Lin, B. Yuan, H. Hong, H. Li, L. He, H. Lu, J. Liu, C. Yan, Post COVID-19 pandemic: Disposable face masks as a potential vector of antibiotics in freshwater and seawater, Sci. Total Environ. (2022) 153049. https://doi.org/10.1016/j.scitotenv.2022.153049.

[24] I. Ioannidis, I. Anastopoulos, I. Pashalidis, Single-use surgical face masks as radionuclide (U-232 and Ra-226) carriers, J. Mol. Liq. 342 (2021), 117578, https://doi.org/10.1016/j.molliq.2021.117578.

[25] K. Qi, N. Lu, S. Zhang, W. Wang, Z. Wang, J. Guan, Uptake of Pb(II) onto microplastic-associated biofilms in freshwater: Adsorption and combined toxicity in comparison to natural solid substrates, J. Hazard. Mater. 411 (2021), 125115, https://doi.org/10.1016/j.jhazmat.2021.125115.

[26] M. Shen, B. Song, G. Zeng, Y. Zhang, F. Teng, C. Zhou, Surfactant changes lead adsorption behaviors and mechanisms on microplastics, Chem. Eng. J. 405 (2021), 126989, https://doi.org/10.1016/j.cej.2020.126989.

[27] Y. Zhou, Y. Yang, G. Liu, G. He, W. Liu, Adsorption mechanism of cadmium on microplastics and their desorption behavior in sediment and gut environments: The roles of water pH, lead ions, natural organic matter and phenanthrene, Water Res. 184 (2020), 116209, https://doi.org/10.1016/j.watres.2020.116209.

[28] I. Mironyuk, T. Tatarchuk, H. Vasylyeva, M. Naushad, I. Mykytyn, Adsorption of Sr (II) cations onto phosphated mesoporous titanium dioxide: Mechanism, isotherm and kinetics studies, J. Environ. Chem. Eng. 7 (2019) 103430. .

[29] X. Guo, J. Wang, The phenomenological mass transfer kinetics model for Sr2+ sorption onto spheroids primary microplastics, Environ. Pollut. 250 (2019) 737–745, https://doi.org/10.1016/j.envpol.2019.04.091.

[30] M.A. Salam, M. Mokhtar, S.M. Albukhari, D.F. Baamer, L. Palmisano, M. R. Abukhadra, Insight into the role of the zeolitization process in enhancing the adsorption performance of kaolinite/diatomite geopolymer for effective retention of Sr (II) ions; batch and column studies, J. Environ. Manage. 294 (2021), 112984, https://doi.org/10.1016/j.jenvman.2021.112984.

[31] Y. Kyung, C. Romera-castillo, S. Hong, J. Hur, Characteristics of microplastic polymer-derived dissolved organic matter and its potential as a disinfection byproduct precursor, Water Res. 175 (2020), 115678, https://doi.org/10.1016/j.watres.2020.115678.

[32] M.C. Zenobi, E.H. Rueda, Adsorption of Me(II), HEDP, and Me(II)-HEDP onto boehmite at nonstoichiometric Me(II)-HEDP concentrations, Environ. Sci. Technol. 40 (2006) 3254–3259, https://doi.org/10.1021/es0519132.

[33] Y. Yan, F. Zhu, C. Zhu, Z. Chen, S. Liu, C. Wang, C. Gu, Dibutyl phthalate release from polyvinyl chloride microplastics: Influence of plastic properties and environmental factors, Water Res. 204 (2021), 117597, https://doi.org/10.1016/j.watres.2021.117597.

[34] H. Li, F. Wang, J. Li, S. Deng, S. Zhang, Adsorption of three pesticides on polyethylene microplastics in aqueous solutions: Kinetics, isotherms, thermodynamics, and molecular dynamics simulation, Chemosphere. 264 (2021), 128556, https://doi.org/10.1016/j.chemosphere.2020.128556.

[35] X.S. Wang, Cd (II) removal by marine Arthrobacter protophormiae biomass: Mechanism characterization and adsorption performance, Desalin. Water Treat. 51 (2013) 7710–7720, https://doi.org/10.1080/19443994.2013.781964.

[36] P. Liu, L. Qian, H. Wang, X. Zhan, K. Lu, C. Gu, S. Gao, New Insights into the Aging Behavior of Microplastics Accelerated by Advanced Oxidation Processes, Environ. Sci. Technol. 53 (2019) 3579–3588, https://doi.org/10.1021/acs.est.9b00493.

[37] C. Shan, Y. Liu, Y. Huang, B. Pan, Non-radical pathway dominated catalytic oxidation of As(III) with stoichiometric H2O2 over nanoceria, Environ. Int. 124 (2019) 393–399, https://doi.org/10.1016/j.envint.2019.01.014.

[38] Y. Muñoz-González, R. Arriagada-Acuña, G. Soto-Garrido, R. García-Lovera, Activated carbons from peach stones and pine sawdust by phosphoric acid activation used in clarification and decolorization processes, J. Chem. Technol. Biotechnol. 84 (2009) 39–47, https://doi.org/10.1002/jctb.2001.

[39] G. Ding, C. Jing, X. Qin, Y. Gong, X. Zhang, Dyes and Pigments Conjugated dyes carrying N, N -dialkylamino and ketone groups : One-component visible light Norrish type II photoinitiators, Dye. Pigment. 137 (2017) 456–467, https://doi.org/10.1016/j.dyepig.2016.10.034.

[40] R. Mao, M. Lang, X. Yu, R. Wu, X. Yang, X. Guo, Aging mechanism of microplastics with UV irradiation and its effects on the adsorption of heavy metals, J. Hazard. Mater. 393 (2020), 122515, https://doi.org/10.1016/j.jhazmat.2020.122515.

[41] G. Liu, Z. Zhu, Y. Yang, Y. Sun, F. Yu, J. Ma, Sorption behavior and mechanism of hydrophilic organic chemicals to virgin and aged microplastics in freshwater and seawater, Environ. Pollut. 246 (2019) 26–33, https://doi.org/10.1016/j.envpol.2018.11.100.

[42] S. Tang, L. Lin, X. Wang, A. Yu, X. Sun, Interfacial interactions between collected nylon microplastics and three divalent metal ions (Cu (II), Ni (II), Zn (II)) in aqueous solutions, J. Hazard. Mater. 403 (2021), 123548, https://doi.org/10.1016/j.jhazmat.2020.123548.

[43] S. Tang, L. Lin, X. Wang, A. Feng, X. Feng, J. Kong, Kinetics of Cu(II) and fulvic acid adsorption on modified biochar derived from rice husk, 189 (2020) 305–315. .

[44] X.S. Wang, L. Zhu, H.J. Lu, Surface chemical properties and adsorption of Cu (II) on nanoscale magnetite in aqueous solutions, Desalination. 276 (2011) 154–160, https://doi.org/10.1016/j.desal.2011.03.040.

[45] G. Bhagwat, T.K.A. Tran, D. Lamb, K. Senathirajah, I. Grainge, W. O'Connor, A. Juhasz, T. Palanisami, Biofilms Enhance the Adsorption of Toxic Contaminants on Plastic Microfibers under Environmentally Relevant Conditions, Environ. Sci. Technol. 55 (2021) 8877–8887, https://doi.org/10.1021/acs.est.1c02012.

[46] X. Li, Q. Mei, L. Chen, H. Zhang, B. Dong, X. Dai, C. He, J. Zhou, Enhancement in adsorption potential of microplastics in sewage sludge for metal pollutants after the wastewater treatment process, Water Res. 157 (2019) 228–237, https://doi.org/10.1016/j.watres.2019.03.069.

[47] D.W. Barnum, Hydrolysis of Cations. Formation Constants and Standard Free Energies of Formation of Hydroxy Complexes, Inorg. Chem. 22 (1983) 2297–2305. https://doi.org/10.1021/ic00158a016.

[48] J. Pan, B. Gao, K. Guo, Y. Gao, X. Xu, Q. Yue, Insights into selective adsorption mechanism of copper and zinc ions onto biogas residue-based adsorbent: Theoretical calculation and electronegativity difference, Sci. Total Environ. 805 (2022), 150413, https://doi.org/10.1016/j.scitotenv.2021.150413.

[49] J. Zou, X. Liu, D. Zhang, X. Yuan, Adsorption of three bivalent metals by four chemical distinct microplastics, Chemosphere. 248 (2020), 126064, https://doi.org/10.1016/j.chemosphere.2020.126064.

[50] S. Yang, C. Chen, Y. Chen, J. Li, D. Wang, X. Wang, W. Hu, Competitive adsorption of PbII, NiII, and SrII ions on graphene oxides: A combined experimental and theoretical study, Chempluschem. 80 (2015) 480–484, https://doi.org/10.1002/cplu.201402284.

[51] Y.K. Lee, J. Hur, Adsorption of microplastic-derived organic matter onto minerals ☆, Water Res. 187 (2020), 116426 https://doi.org/10.1016/j.watres.2020.116426.

[52] L.A. Holmes, A. Turner, R.C. Thompson, Interactions between trace metals and plastic production pellets under estuarine conditions, Mar. Chem. 167 (2014) 25–32, https://doi.org/10.1016/j.marchem.2014.06.001.

[53] E.R. Nightingale, Phenomenological theory of ion solvation. Effective radii of hydrated ions, J. Phys. Chem. 63 (9) (1959) 1381–1387.

[54] F. Wang, W. Yang, P. Cheng, S. Zhang, S. Zhang, W. Jiao, Y. Sun, Adsorption characteristics of cadmium onto microplastics from aqueous solutions, Chemosphere. 235 (2019) 1073–1080, https://doi.org/10.1016/j.chemosphere.2019.06.196.

[55] S. Tang, L. Lin, X. Wang, A. Feng, A. Yu, Pb(II) uptake onto nylon microplastics: Interaction mechanism and adsorption performance, J. Hazard. Mater. 386 (2020), 121960, https://doi.org/10.1016/j.jhazmat.2019.121960.

[56] Q. Fu, X. Tan, S. Ye, L. Ma, Y. Gu, P. Zhang, Q. Chen, Y. Yang, Y. Tang, Chemosphere Mechanism analysis of heavy metal lead captured by natural-aged microplastics, Chemosphere. 270 (2021), 128624, https://doi.org/10.1016/j.chemosphere.2020.128624.

[57] L. Lin, S. Tang, X. Wang, X. Sun, A. Yu, Hexabromocyclododecane alters malachite green and lead(II) adsorption behaviors onto polystyrene microplastics: Interaction mechanism and competitive effect, Chemosphere. 265 (2021), 129079, https://doi.org/10.1016/j.chemosphere.2020.129079.

[58] Y. Dong, M. Gao, Z. Song, W. Qiu, Adsorption mechanism of As(III) on polytetrafluoroethylene particles of different size, Environ. Pollut. 254 (2019), 112950, https://doi.org/10.1016/j.envpol.2019.07.118.

[59] B.H.W.S. De Jong, D. Ellerbroek, A.L. Spek, Low-temperature structure of lithium nesosilicate, Li4SiO4, and its Li1s and O1s X-ray photoelectron spectrum, Acta Crystallogr. Sect. B. 50 (1994) 511–518, https://doi.org/10.1107/S0108768194002375.

[60] Y. Dong, M. Gao, Z. Song, W. Qiu, As(III) adsorption onto different-sized polystyrene microplastic particles and its mechanism, Chemosphere. 239 (2020), 124792, https://doi.org/10.1016/j.chemosphere.2019.124792.

[61] C. Shan, H. Liu, M. Hua, B. Pan, Enhanced Fenton-like Oxidation of As(III) over Ce-Ti Binary Oxide: A New Strategy to Tune Catalytic Activity via Balancing Bimolecular Adsorption Energies, Environ. Sci. Technol. 54 (2020) 5893–5901, https://doi.org/10.1021/acs.est.0c00159.

[62] Y. Wang, X. Wang, Y. Li, J. Li, F. Wang, S. Xia, J. Zhao, Biofilm alters tetracycline and copper adsorption behaviors onto polyethylene microplastics, Chem. Eng. J. 392 (2020), 123808, https://doi.org/10.1016/j.cej.2019.123808.

[63] A.L. Patrício Silva, J.C. Prata, C. Mouneyrac, D. Barcelò, A.C. Duarte, T. Rocha-Santos, Risks of Covid-19 face masks to wildlife: Present and future research needs, Sci. Total Environ. 792 (2021), 148505, https://doi.org/10.1016/j.scitotenv.2021.148505.

[64] E. Okuku, L. Kiteresi, G. Owato, K. Otieno, C. Mwalugha, M. Mbuche, B. Gwada, A. Nelson, P. Chepkemboi, Q. Achieng, V. Wanjeri, J. Ndwiga, L. Mulupi, J. Omire, The impacts of COVID-19 pandemic on marine litter pollution along the Kenyan Coast : A synthesis after 100 days following the first reported case in Kenya, Mar. Pollut. Bull. 162 (2021), 111840, https://doi.org/10.1016/j.marpolbul.2020.111840.

[65] M. Reza, I. Suci, E. Riani, Chemosphere Unprecedented plastic-made personal protective equipment (PPE) debris in river outlets into Jakarta Bay during COVID-19 pandemic, Chemosphere. 268 (2021) 129360. https://doi.org/10.1016/j.chemosphere.2020.129360.

[66] J.M. Mumma, E. Jordan, O. Ayeni, N. Kaufman, M.J. Wheatley, A. Grindle, J. Morgan, Development and validation of the discomfort of cloth Masks-12 (DCM-12) scale, Appl. Ergon. 98 (2022), 103616, https://doi.org/10.1016/j.apergo.2021.103616.

[67] L.A. Holmes, A. Turner, R.C. Thompson, Adsorption of trace metals to plastic resin pellets in the marine environment, Environ. Pollut. 160 (2012) 42–48, https://doi.org/10.1016/j.envpol.2011.08.052.

[68] A. Turner, L.A. Holmes, Adsorption of trace metals by microplastic pellets in fresh water, Environ. Chem. 12 (2015) 600–610, https://doi.org/10.1071/EN14143.

[69] V. Godoy, G. Blázquez, M. Calero, L. Quesada, M.A. Martín-Lara, The potential of microplastics as carriers of metals, Environ. Pollut. 255 (2019). .

[70] M. Lang, X. Yu, J. Liu, T. Xia, T. Wang, H. Jia, X. Guo, Fenton aging significantly affects the heavy metal adsorption capacity of polystyrene microplastics, Sci. Total Environ. 722 (2020), 137762, https://doi.org/10.1016/j.scitotenv.2020.137762.

[71] X. Guo, G. Hu, X. Fan, H. Jia, Sorption properties of cadmium on microplastics: The common practice experiment and A two-dimensional correlation spectroscopic study, Ecotoxicol. Environ. Saf. 190 (2020), 110118, https://doi.org/10.1016/j.ecoenv.2019.110118.

[72] X. Guo, Y. Liu, J. Wang, Equilibrium, kinetics and molecular dynamic modeling of Sr 2 + sorption onto microplastics, J. Hazard. Mater. 400 (2020), 123324, https://doi.org/10.1016/j.jhazmat.2020.123324.